2023-01-1600 Published 31 Oct 2023

Model Free Time Delay Compensation for Damped Impedance Method Interfaced Power System Co-Simulation Testing

Elutunji Buraimoh, Gokhan Ozkan, Laxman Timilsina, Ali Arsalan, Behnaz Papari, Phani Kumar Chamarthi, and Christopher Edrington Clemson University

Citation: Buraimoh, E., Ozkan, G., Timilsina, L., Arsalan, A. et al., "Model Free Time Delay Compensation for Damped Impedance Method Interfaced Power System Co-Simulation Testing," SAE Technical Paper 2023-01-1600, 2023, doi:10.4271/2023-01-1600.

Received: 15 Jun 2023 Revised: 19 Aug 2023 Accepted: 24 Aug 2023

Abstract

The joint real-time co-simulation, which involves the virtual integration of laboratories located in different locations, is met with challenges, especially the communication latency or delay, which significantly affects co-simulation accuracy and system stability. The real-time power system co-simulation is particularly susceptible to these delays and could lose synchronism, which affects the simulation fidelity and limits dynamic and transient studies. This paper proposes a model-free framework for predicting and compensating delays in the virtual integration of real-time co-simulators through the damped impedance interface method to address this issue. The framework includes an improved co-simulation interface algorithm called the Damping Impedance Method (DIM) and a model-free predictor system designed to predict and compensate for delays without decomposing and reconstructing signals at coupling points. The predictor systems use one design parameter and two design parameters to achieve delay compensation through a first-order time delay compensation system. The framework enhances the accuracy and stability of the system, making it suitable for dynamic and transient studies.

Introduction

Virtual integration of real-time digital simulators, Hardware-in-the-loop (HIL), Power Hardware-in-the-Loop (PHIL), and Controller Hardware-in-the-Loop (CHIL) across long geographical distances refers to the ability to connect and operate multiple simulators in different locations as if they were a single integrated system. This concept is used in various fields, such as power systems [1], aerospace, and automotive engineering [2] to simulate complex systems and test their behavior in different scenarios [3]. A "power system" denotes a complex and interconnected network comprising generation, transmission, and distribution components, designed to efficiently generate, transmit, and deliver electrical energy to consumers. This infrastructure integrates various sources, such as power plants and renewable resources, alongside control mechanisms to maintain reliable and stable electricity supply, accommodating diverse demand scenarios while adhering to operational, economic, and regulatory constraints [4]. The idea behind virtual integration is to leverage high-speed data communication networks to enable real-time communication between simulators in different locations. This allows engineers and operators to test and validate complex systems in a more realistic environment without the need for physical prototypes or expensive testing facilities [5].

HIL is a real-time simulation technique used in engineering and testing processes. HIL involves integrating physical hardware components with computer-based simulations to assess and validate the performance of complex systems. PHIL extends the HIL concept specifically to power systems and electronics. PHIL focuses on the integration of physical power equipment, such as inverters, converters, or generators, with virtual models to analyze and optimize power-related components and control strategies. CHIL is a specialized form of HIL that emphasizes the validation of control algorithms and software modules. CHIL involves connecting physical controllers or embedded systems to simulation environments to assess their performance in real-time scenarios.

To achieve virtual integration, real-time digital simulators must be designed to communicate over network protocols, such as the Internet Protocol (IP). The simulators must also be synchronized in time to ensure consistent simulation results across all locations [6]. There are several advantages to virtual integration. First, it allows for more efficient and cost-effective testing of complex systems [7]. Second, it enables engineers to collaborate and share resources across different locations, which can improve overall productivity [6]. Finally, it provides a more realistic testing environment, which can lead to better performance and increased safety in real-world applications [8, 9].

The virtual integration of software and hardware assets in different locations has recently attracted much research interest. However, realizing joint real-time simulation in virtually connected laboratories has challenges, including communication latency. Latency is the delay between the sending of signals collected from a real-time simulator and the receiving process that gives the signal received to the remote real-time simulator's solver to complete the entire system's numerical calculation [5]. Delay is primarily responsible for instability and inaccuracy in networked real-time co-simulation; thus, the effect of latency must be minimized by applying particular solutions. Moreover, the power system, most especially, is susceptible to these delays and could lose synchronism which could affect the simulation fidelity, thereby making it not eligible for dynamic and transient studies.

Furthermore, virtual integration also presents some challenges. For example, it requires high-bandwidth [6], low-latency communication networks to ensure real-time communication between simulators. It also requires sophisticated synchronization algorithms to ensure consistent simulation results across all locations [10]. Despite these challenges, virtual integration of real-time digital simulators is becoming increasingly popular in many industries. As technology continues to advance, it is likely that we will see more widespread adoption of this concept in the future [11].

Latency or delay is a critical factor in networked real-time co-simulation, and it can lead to system instability and inaccuracy in the simulation results. In the case of power systems, which are highly dynamic and complex, delays can have a significant impact on the simulation accuracy, making it unsuitable for dynamic and transient studies [12, 13]. To minimize the effect of latency in networked real-time co-simulation, several solutions can be applied, such as: Using high-speed networks with low latency, such as fiber-optic networks, can reduce the delay and improve the accuracy of the simulation [5]. Synchronizing the clocks of the simulators to a common reference time can help to minimize the effect of latency on the simulation results. Parallelizing the simulation across multiple processors or computers can help to reduce the computational load and improve the simulation performance [6]. Prediction algorithms: Using prediction algorithms to estimate the system's future state can help compensate for the latency and improve the accuracy of the simulation [14]. Using co-simulation frameworks specifically designed to handle networked simulations can help reduce the effect of latency and improve the accuracy of the simulation.

Consequently, minimizing the effect of latency is crucial to ensuring the accuracy and stability of networked real-time co-simulation, especially in the case of power systems, where simulation fidelity is critical for dynamic and transient studies. This work aims to develop a framework for delay compensation and predicting delays in the virtual integration of real-time co-simulators in laboratories/facilities at different locations. Typically, most co-simulation interface algorithms (IAs) are based on the ideal transformer model (ITM), which uses controlled voltage and current sources to impose the remote subsystem's behavior on the local subsystems; however, ITM's stability and accuracy are highly compromised in the presence of delay. Thus, an improved IA called the Damping Impedance Method (DIM), based on the calculation of the second subsystem equivalent impedance, is included in the interface to enhance system accuracy and stability. Furthermore, a one-parameter and two-parameter model-free predictor framework is deployed in predicting and compensating for network delays in power systems partitioned by the DIM. The predictor is designed as a first-order-time delay compensation system with one and two design parameters. The delay compensation is achieved without the decomposition and reconstruction of the signals at the coupling points.

System's Interface Algorithm

The interfaces deployed to monolithic PHIL also apply in the virtual coupling and integration of geographically dispersed real-time co-simulation experiment. There are several co-simulation interface algorithms (IAs) listed in the literature, including the Ideal Transformer Model (ITM) algorithm, Advanced ITM (AITM), Time-Variant First-order Approximation (TFA) algorithm, Transmission Line Model (TLM) algorithm, Partial Circuit Duplication (PCD) method, DIM, and IA Extendible Feedback Current Filter [15]. A good IA should increase the accuracy and stability of the co-simulation while ensuring interaction between the subsystems simulated in two different simulations [16]. Additionally, a good IA should have low computational cost, robustness, flexibility, scalability and accuracy. Thus, selecting the right IA is critical to ensuring the co- simulation's accuracy, stability, and efficiency. Different IAs may be suitable for different simulation scenarios, depending on the characteristics of the subsystems and the simulation environment. Therefore, carefully considering and evaluating the different IAs are essential to selecting the most appropriate one for a given co-simulation scenario.

The ideal transformer model (ITM) is a common co-simulation interface algorithm (IA) used to connect different subsystems in a co-simulation environment. The ITM uses controlled voltage and current sources to impose the remote subsystem's behavior on the local subsystems [17]. However, the stability and accuracy of the ITM can be compromised in the presence of delay. This is because the ITM assumes that the transmission delay is zero, and any delay can cause errors in the simulation results. As a result, the ITM is not suitable for real-time co-simulation environments, where latency is a critical factor [17]. The ITM transfer function is given in (1) where Figure 1 indicates the range of operation of ITM in which the criteria for Nyquist is violated when the ratio of impedance of subsystem 1 to subsystem 2 exceeds 1.

To address this issue, several alternative co-simulation interface algorithms have been developed. The DIM incorporates an extra impedance optimizing the convergence factor, enhancing the precision and stability of the Partial Circuit Duplication algorithm. The PCD transfer function is given in (2) while the corresponding range of operation is given in Figure 2. Figure 2 in this context suggests that the system can remain stable even when the coupling impedance is small. However, adding more impedances to the partitioned

FIGURE 1 ITM range of operation.

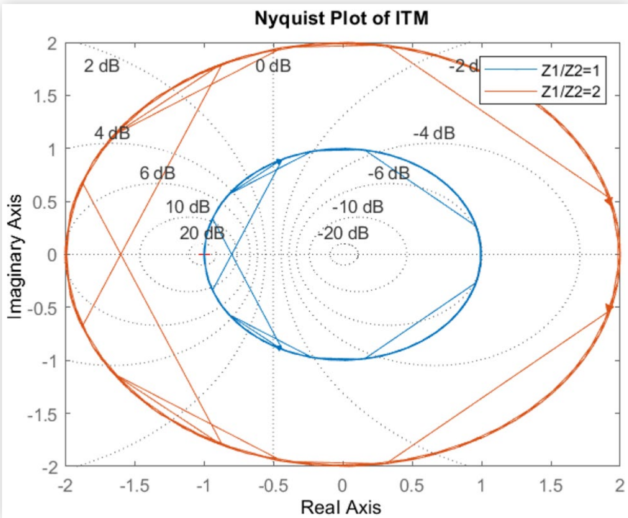

FIGURE 2 PCD range of operation.

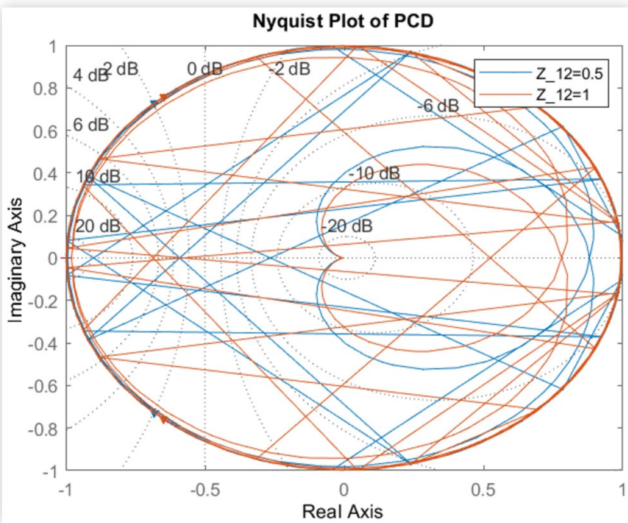

subsystems can increase the influence on the co-simulation outcomes. This is because the power consumption of the additional components can also affect the overall results of the simulation.

$$G_0 = \frac{Z_1(s)}{Z_2(s)} e^{-s\Delta t} \tag{1}$$

$$G_0 = \frac{Z_1(s) Z_2(s)}{\left[Z_1(s) + Z_{12}(s)\right]\left[Z_2(s) + Z_{12}(s)\right]} e^{-s\Delta t} \tag{2}$$

$$G_0 = \frac{Z_1(s)\left[Z_2(s) - Z*(s)\right]}{\left[Z_1(s) + Z_{12}(s)\right]\left[Z_2(s) + Z_{12}(s) + Z*(s)\right]} e^{-s\Delta t} \tag{3}$$

FIGURE 3 Interface Algorithm: Damping Impedance Method.

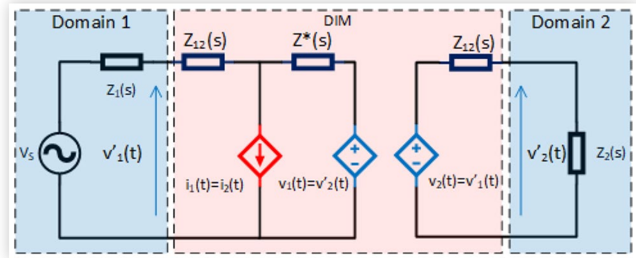

The DIM is a hybrid of the PCD and ITM algorithm and is achieved by placing a damp impedance, Z*, between current and voltage sources. The DIM transfer function is given in (3), and it is evident that when Z* approaches infinity, the DIM assumes the ITM arrangement, but when Z* approaches zero value, it assumes the PCD configuration. The implemented DIM IA is shown in Figure 3 while the corresponding Nyquist plot is given in Figure 4. Figure 4 is the range of operation of the DIM IA system. This range is wider than what other methods earlier provided. The graph shows that when the coupling impedance (Z*) is equal to the characteristic impedance, there is no increase in the number of stable conditions. However, if Z* is much greater or much smaller than subsystem 1impedance, the system can become unstable. The DIM technique alternates between the PCD and ITM methods with Z*, as confirmed in Figure 3; thus, its stability significantly rests on the estimate of Z*. Absolute stability is ensured when Z* matches subsystem 2 impedance. Consequently, the DIM is more stable than the ITM and PCD methods and is computationally efficient.

The DIM interface connects the subsystems with a current and two voltage sources. The voltage sources are controlled by the voltage output of the remote subsystems, while the current output of local subsystem 2 regulates the current source in subsystem 1. The damping impedance is placed between the current and voltage sources of subsystem 1.

FIGURE 4 DIM range of operation.

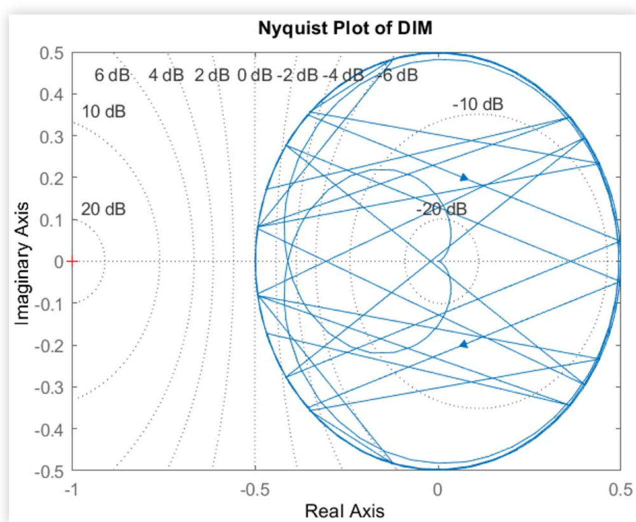

System's Interface Signal Delay Compensation

Two different predictors are introduced for the closed-loop coupling variables to accurately predict a complex power system's behavior. In the case of the DIM interface configuration depicted in Figure 5, two observers that predict subsystem 2's undelayed coupling signals are implemented on subsystem 1 for the voltage and current control signals of the controlled voltage and current sources, respectively. Also, one observer that predicts subsystem 1's undelayed coupling signals is used on subsystem 2 for the voltage signal. Using these multiple predictors allows for the simultaneous prediction of multiple system variables, resulting in a more comprehensive understanding of the system's behavior.

The predictor for this interface is developed from the principle of sliding mode control [18, 19, 20]. The sliding mode control is a control strategy that is used to simplify the control of complex systems to that of a first-order system. It achieves this by defining a specific surface, known as a sliding surface, in the system's phase space, and using the input of control that influences the system to slide along that surface [18]. Phase space is a multidimensional space where each dimension represents a state variable of a dynamic system. This approach is a non-linear control technique and offers several advantages over traditional control methods, such as robustness to disturbances, uncertainties in system parameters, and unmodeled dynamics [20]. The ability to tolerate these factors makes sliding mode control an attractive option for controlling complex systems where traditional linear control techniques may be insufficient. Despite disturbances, the sliding mode control achieves fast convergence to the desired state, and the implementation is straightforward. However, the control signal's discontinuity can induce chattering, characterized by high-frequency system oscillations, which is undesirable in precision-critical applications. Thus, the optimal selection of sliding mode controller gain ensures convergence without chattering since excessive gain leads to chattering while insufficient gain hinders desired state convergence.

Considering a single input system with a non-linear structure, which can be mathematically represented using equation (4) where scalars $x(t)^n$ and $u(t)$ represent the system's state desired output and the system's inputs. The vector $x(t)$ is the state vector while functions $f(x(t))$ and $g(x(t))$ are non-linear. The function $f(x(t))$ is unknown, yet the imprecision in $f(x(t))$ remains bounded by an established continuous function dependent on $x(t)$. Likewise, the control gain $g(x(t))$, while not precisely determined, maintains a known sign and is constrained by identifiable, continuous functions of $x(t)$. Equation (4) provides a model for the system's behavior and can be used to understand the system's dynamics.

FIGURE 5 Damping Impedance Method with Implemented Predictors.

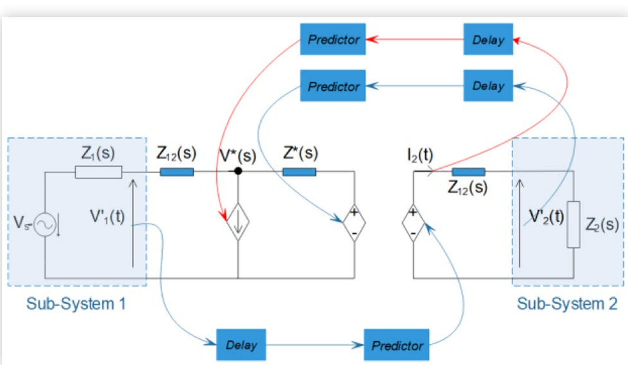

$$x(t)^n = f\big(x(t)\big) + g\big(x(t)\big).u(t) \tag{4}$$

The system under consideration can be described by equation (4), where the state scalar $x(t)^n$ represents the system states relevant to the computation of the coupling signals exchanged at the virtual interface, and $u(t)$ represents the system inputs. Both of these components are essential to the overall behavior of the system. The two non-linear functions $f(x(t))$ and $g(x(t))$ govern the system's dynamics and interactions. Non-linear functions can be challenging to analyze and predict due to their nonlinearity, but they are necessary for modeling systems that exhibit complex behaviors [21, 22]. However, with mathematical models and appropriate analysis techniques, it is possible to gain insight into the behavior of these systems. Control of the system's inputs and outputs to achieve desired performance specifications through appropriate mathematical techniques, such as sliding mode control, is possible. The ability to control non-linear systems is essential in various applications, including robotics, aerospace engineering, and power systems.

The system represented by equation (4) can be analyzed using sliding mode control, to ensure that it operates optimally and satisfies performance specifications [19, 20]. Equations (5), (6), and (7) define respective sliding surfaces, respectively defined in the two-dimensional phase plane for the three error systems ($e_{v1}(t)$, $e_{i2}(t)$, and $e_{v2}(t)$) of three control signals for the controlled voltage source 1 ($v_1(t)$), the controlled current source ($i_2(t)$), and the controlled voltage source 2 ($v_2(t)$).

$$\left(\alpha + \frac{d}{dt}\right) e_{v1}(t) = 0 \tag{5}$$

$$\left(\alpha + \frac{d}{dt}\right) e_{i2}(t) = 0 \tag{6}$$

$$\left(\alpha + \frac{d}{dt}\right) e_{v2}(t) = 0 \tag{7}$$

The parameter α determines the surface's slope for the three error systems. Another term $\beta \frac{d}{dt}$ can be added to the error system multiplier $\left(\alpha + \frac{d}{dt}\right)$ in the sliding surface such that parameters α and β both determine the surface's slope with higher degrees of freedom. This technique can establish a model-based observer by using a local model of the remote system in the local site, and a sliding mode control makes the model's states closely match those of the remote system [18, 19, 20]. This design differs from previous approaches in that it employs the concept of a sliding surface to develop a dynamic equation for a predictor that does not rely on a predetermined model of the remote system. The aim is to use the sliding surface as a basis for developing a predictor that can accurately track the actual state of the remote system without being limited by the assumptions or limitations of a model-based approach. Consequently, the state tracking errors between the predictor states $\hat{v}_1(t)$, $\hat{i}_2(t)$, and $\hat{v}_2(t)$ and the initially sent state of the remote system $v_1(t)$, $i_2(t)$, and $v_2(t)$ are given in (8), (9), and (10)

$$e_{v1}(t) = v_1(t) - \hat{v}_1(t) \tag{8}$$

$$e_{i2}(t) = i_2(t) - \hat{i}_2(t) \tag{9}$$

$$e_{v2}(t) = v_2(t) - \hat{v}_2(t) \tag{10}$$

Equations (11), (12), and (13) can be used to derive a dynamic equation for the observer state to keep the error system on the sliding surface when there are no communication delays. Recall that within the context of this article and the DIM interface algorithm, subsystem 1 incorporates an observer dedicated to subsystem 2, and subsystem 2 incorporates two observers dedicated to subsystem 1. The primary objective of this observer is to predict the immediate response of Subsystem 2 to the influence exerted by Subsystem 1 and vice versa without accounting for any delays.

$$\frac{d\left[\hat{v}_1(t)\right]}{dt} = \frac{d\left[v_1(t)\right]}{dt} + \alpha\left[v_1(t) - \hat{v}_1(t)\right] + \beta\frac{d\left[v_1(t) - \hat{v}_1(t)\right]}{dt} \tag{11}$$

$$\frac{d\left[\hat{i}_2(t)\right]}{dt} = \frac{d\left[i_2(t)\right]}{dt} + \alpha\left[i_2(t) - \hat{i}_2(t)\right] + \beta\frac{d\left[i_2(t) - \hat{i}_2(t)\right]}{dt} \tag{12}$$

$$\frac{d\left[\hat{v}_2(t)\right]}{dt} = \frac{d\left[v_2(t)\right]}{dt} + \alpha\left[v_2(t) - \hat{v}_2(t)\right] + \beta\frac{d\left[v_2(t) - \hat{v}_2(t)\right]}{dt} \tag{13}$$

In reality, however, the remote signals $v_1(t)$, $i_2(t)$, and $v_2(t)$ and $\frac{d\left[v_1(t)\right]}{dt}$, $\frac{d\left[i_2(t)\right]}{dt}$, and $\frac{d\left[v_2(t)\right]}{dt}$ are available only with a delay. Thus, Equations (11), (12), and (13) become (14), (15), and (16) where the remote signals specified with delays, respectively. Recall that the remote signal $v_1(t)$ is the signal sent from Subsystem 1 to Subsystem 2 while remote signals $i_2(t)$ and $v_2(t)$ are the signals sent from Subsystem 2 to Subsystem 1.

$$\frac{d\left[\hat{v}_1(t)\right]}{dt} = \frac{d\left[v_1(t-\tau)\right]}{dt} + \alpha\left[v_1(t-\tau) - \hat{v}_1(t)\right] + \beta\frac{d\left[v_1(t-\tau) - \hat{v}_1(t)\right]}{dt} \tag{14}$$

$$\frac{d\left[\hat{i}_2(t)\right]}{dt} = \frac{d\left[i_2(t-\tau)\right]}{dt} + \alpha\left[i_2(t-\tau) - \hat{i}_2(t)\right] + \beta\frac{d\left[i_2(t-\tau) - \hat{i}_2(t)\right]}{dt} \tag{15}$$

$$\frac{d\left[\hat{v}_2(t)\right]}{dt} = \frac{d\left[v_2(t-\tau)\right]}{dt} + \alpha\left[v_2(t-\tau) - \hat{v}_2(t)\right] + \beta\frac{d\left[v_2(t-\tau) - \hat{v}_2(t)\right]}{dt} \tag{16}$$

where the second and the third terms on the right-hand side of (14). (15), and (16) are differences in the delayed states $v_1(t-\tau)$, $i_2(t-\tau)$, and $v_2(t-\tau)$, and the predicted states $\hat{v}_1(t)$, $\hat{i}_2(t)$, and $\hat{v}_2(t)$. However, This would result in the designed predictor following the delayed remote states $v_1(t-\tau)$, $i_2(t-\tau)$, and $v_2(t-\tau)$ instead of the current remote states $v_1(t)$, $i_2(t)$, and $v_2(t)$ and making the prediction irrelevant. Additionally, the expressions $v_1(t-\tau) - \hat{v}_1(t)$, $i_2(t-\tau) - \hat{i}_2(t)$, and $v_2(t-\tau) - \hat{v}_2(t)$, when comparing states that belong to different time instances, it is not appropriate to call them "state errors". Therefore, in order to define an error that is more meaningful and useful, an alternative approach is required; thus, the equations (14), (15) and (16) need to be modified to account for the delay in the predictor states. This modification will result in the predictor designs given by equations (17), (18), and (19). The changes made in the equations will delay the predictor states, allowing them to track the states of the remote system accurately.

$$\frac{d\left[\hat{v}_1(t)\right]}{dt} = \frac{d\left[v_1(t-\tau)\right]}{dt} + \alpha\left[v_1(t-\tau) - \hat{v}_1(t-\tau)\right] + \beta\frac{d\left[v_1(t-\tau) - \hat{v}_1(t-\tau)\right]}{dt} \tag{14}$$

$$\frac{d\left[\hat{i}_2(t)\right]}{dt} = \frac{d\left[i_2(t-\tau)\right]}{dt} + \alpha\left[i_2(t-\tau) - \hat{i}_2(t-\tau)\right] + \beta\frac{d\left[i_2(t-\tau) - \hat{i}_2(t-\tau)\right]}{dt} \tag{15}$$

$$\frac{d\left[\hat{v}_2(t)\right]}{dt}=\frac{d\left[v_2(t-\tau)\right]}{dt}+\alpha\left[v_2(t-\tau)-\hat{v}_2(t-\tau)\right]+\beta\frac{d\left[v_2(t-\tau)-\hat{v}_2(t-\tau)\right]}{dt} \quad (16)$$

The output function of the observer as given in (14), (15), and (16) give an estimation of the non-delayed state of the subsystem in remote site, $\hat{v}_1(t)$, $\hat{i}_2(t)$, and $\hat{v}_2(t)$. The observer obtained after modifying equations (14), (15), and (16) to include delays is a first-order system with a time delay. This time delay system is designed using the parameters α and β. However, when β is zero, the prediction system becomes a single parameter predictor with less degree of freedom. Assuming all the terms on the right-hand side of (14), (15), and (16) are absolutely established, the designed predictors' sole target is to drive its predicted states, $\hat{v}_1(t)$, $\hat{i}_2(t)$, and $\hat{v}_2(t)$, closest to the remote state system, $v_1(t)$, $i_2(t)$, and $v_2(t)$. The predictor design does not require any information about the underlying dynamics of the system. As described in equations (14), (15), and (16), the delay τ can be measured by synchronizing the clocks on both sides of the communication channel and time-stamping the packets. The observer is a first-order time delay system, with the parameters α and β being the only design variables for predicting or estimating the state variables at the current time t.

We can express the transfer function (ratio of the error and coupling error) that corresponds to the system using equations (17) and (18) for a one-parameter and a two-parameter prediction system. According to the theory [18], the parameter β affects system performance differently than the parameter α. Therefore, by using both α and β as tuning parameters, it is possible to increase the number of options available for designing the system. This increased flexibility in design can lead to better overall system performance.

$$\frac{E_{v1}(s)}{C_{v1}(s)}=\frac{E_{i1}(s)}{C_{i1}(s)}=\frac{E_{v2}(s)}{C_{v2}(s)}=\frac{s}{s+\alpha se^{-\tau s}} \quad (17)$$

$$\frac{E_{v1}(s)}{C_{v1}(s)}=\frac{E_{i1}(s)}{C_{i1}(s)}=\frac{E_{v2}(s)}{C_{v2}(s)}=\frac{s}{s+\alpha se^{-\tau s}+\beta e^{-\tau s}} \quad (18)$$

The fact that a predictor is stable does not always mean it can effectively compensate for the delay. In other words, an observer may be stable but not reduce the prediction error below the coupling error. The analysis is done in the frequency domain to examine how well the observer's prediction compensates for the delay, and the expression for it is given below.

The stability margin for the value of α is between 0 and π/2τ [19] for one parameter predictor; thus, the value of α parameter for the purpose of this work is set at 95% of 2π/τ. However, for two parameters, there is a level of flexibility in the choice of the values of the tuning parameters. Figures 6 and 7 keep the values of α and β for 1-parameter and 2-parameter prediction, while different delay values τ are analyzed. The results show that as τ increases, the error gain in the high-frequency region and the overshoot in the medium-frequency region both increase. Furthermore, the bandwidth decreases with an increase in τ. However, the error gain in the low-frequency region and the amplitude of oscillations in the high-frequency region remain unaffected, regardless of the delay τ. For two-parameter prediction, the value of α parameter is reduced to 85% of π/2τ to reduce the oscillation and improve the flexibility of β in two-parameter design.

FIGURE 6 Constant Alpha and Beta at 0.95×2π/τ and 0, respectively.

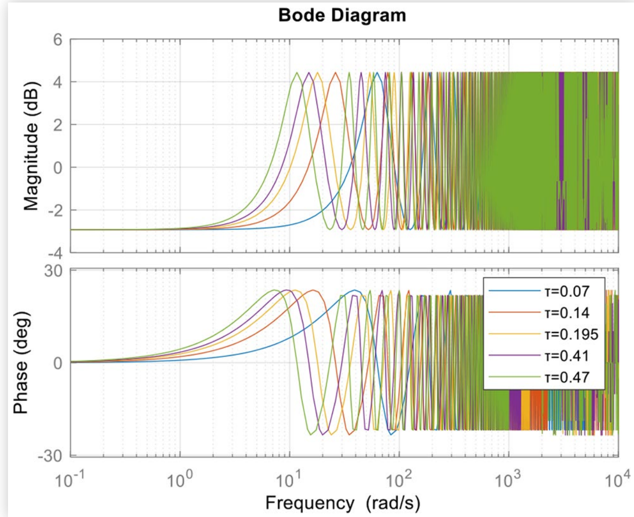

FIGURE 7 Constant Alpha and Beta at 0.8×2π/τ and 0.35, respectively.

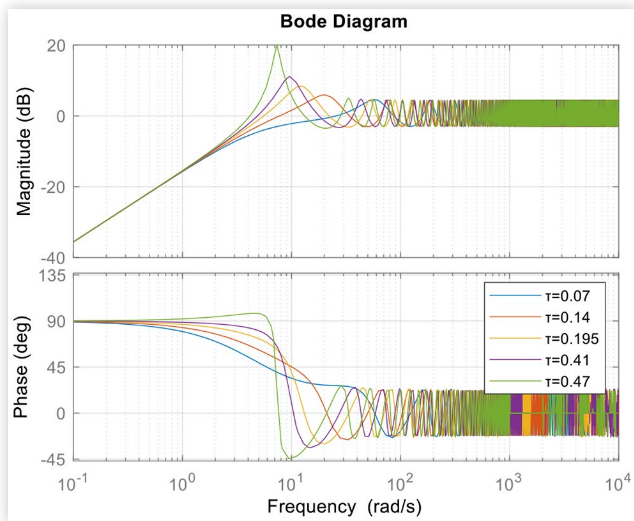

Implementation and Results

Figure 8 illustrates the impact of communication latencies on the coupling signals used as control signals for the controlled voltage source 1 ($v_1(t)$), the controlled current source ($i_2(t)$), and

FIGURE 8 Sent and Received Coupling Signals without prediction under 1ms delay.

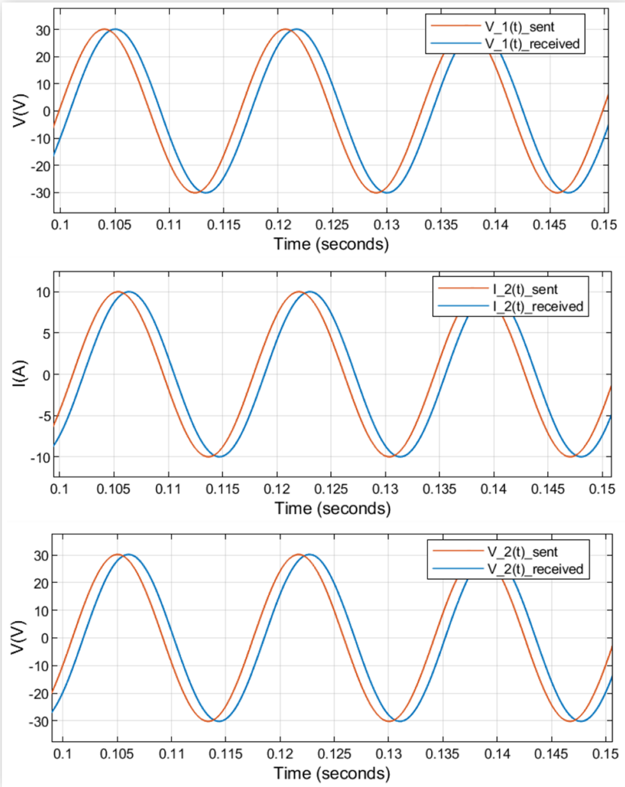

the controlled voltage source 2 ($v_2(t)$). It demonstrates the disparity between the transmitted reference signal and the delayed signal received at any given moment. This phenomenon necessitates the prediction scheme to mitigate the effect of the delay, where coupling signals ($v_1(t)$), ($i_2(t)$), and ($v_2(t)$) exchanged between two simulators indicated a communication latency shift of 1 millisecond between the transmitted and received signals.

Single-parameter and double-parameter model-free predictions are deployed on the three interface or coupling signals of DIM to verify the analysis presented in the previous session and to gain a deeper understanding of the transient behavior of the predictors in the power system application. The purpose is to test the analysis's accuracy and obtain practical insights into the single-parameter and double-parameter predictors' performance in power system applications with a DIM interface. This involves applying the observer's predictions to the control signal of the controlled voltage source 2, the control signal of the controlled current source, and the control signal of the controlled voltage source 1 and measuring their performances. The results obtained validate the theoretical analysis and provide additional information about the three predictors' transient performance. Through case studies, it is possible to gain practical experience and identify potential issues or limitations that may not be apparent through theoretical analysis alone.

This approach is crucial in developing reliable and effective predictors for real-time power system applications. The sent voltage $v_1(t)$ from subsystem 1 and predicted signals $\hat{v}_1(t)$ received in subsystem 2 are shown in Figure 9 and Figure 10 for one-parameter and two-parameter prediction, respectively. The sent current $i_2(t)$ from subsystem 2 and predicted signals $\hat{i}_2(t)$ received in subsystem 1 are shown in Figure 10 and Figure 12 for one-parameter and two-parameter prediction, respectively. Furthermore, the sent voltage $v_2(t)$ from subsystem 2 and predicted signals $\hat{v}_2(t)$ received in subsystem 1 are shown in Figure 13 and Figure 14 for one-parameter and two-parameter prediction, respectively.

The variables $c_{v1}(t)$, $c_{i2}(t)$ and $c_{v2}(t)$ represent the coupling errors caused by communication delay, and it is not considered part of the input to the error prediction system for the three interface signals. The $c_{v1}(t)$, $c_{i2}(t)$ and $c_{v2}(t)$ are given as the difference between the actual undelayed signal and the delayed signal, as a result of the communication delay causing the coupling error. Furthermore, the state tracking errors $e_{v1}(t)$, $e_{i2}(t)$ and $e_{v2}(t)$ are the difference between the actual state of a remote system and the locally predicted version of the same signal.

Figure 15 and Figure 16 illustrate the state tracking error and coupling error for the sent voltage $v_1(t)$ prediction system

FIGURE 9 DIM Voltage 1 Interface Sent and Received Signals after prediction under 1ms delay in 1-Parameter Predictor.

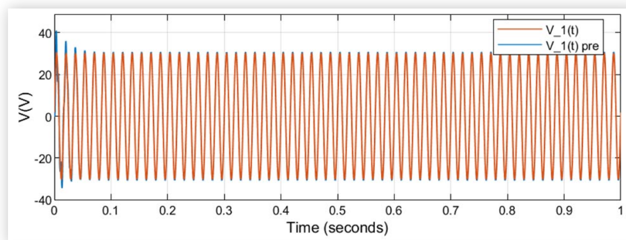

FIGURE 10 DIM Voltage 1 Interface Sent and Received Signals after prediction under 1ms delay in 2-Parameter Predictor.

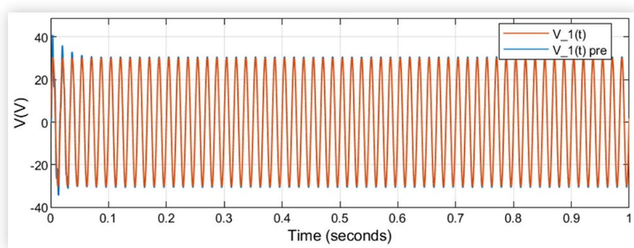

FIGURE 11 DIM Current Interface Sent and Received Signals after prediction under 1ms delay in 1-Parameter Predictor.

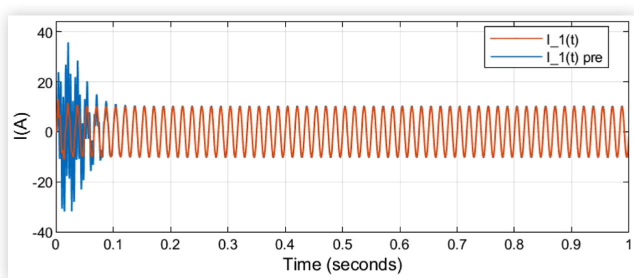

FIGURE 12 DIM Current Interface Sent and Received Signals after prediction under 1ms delay in 2-Parameter Predictor.

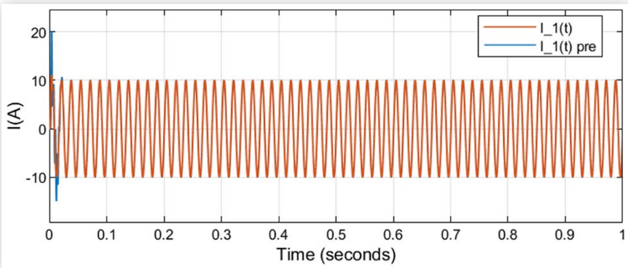

FIGURE 13 DIM Voltage 1 Interface Sent and Received Signals after prediction under 1ms delay in 1-Parameter Predictor.

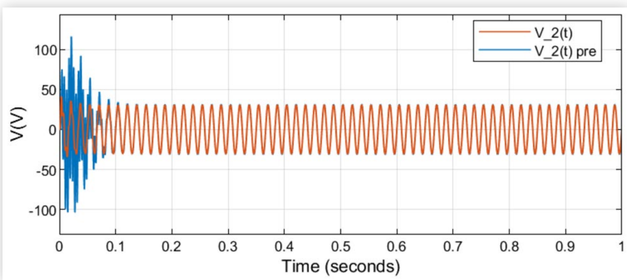

FIGURE 14 DIM Voltage 1 Interface Sent and Received Signals after prediction under 1ms delay in the 2-Parameter predictor.

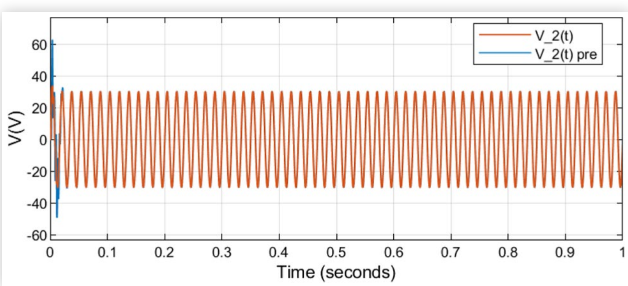

FIGURE 15 State Tracking Error and Coupling Error for Control Signal of the Controlled Voltage Source 1 in 1-Parameter Predictor.

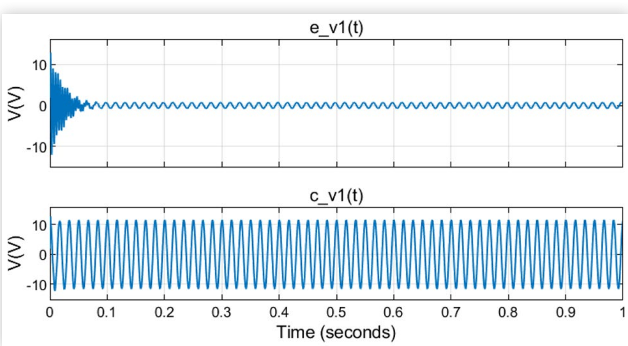

FIGURE 16 State Tracking Error and Coupling Error for Control Signal of the Controlled Voltage Source 1 in 2-Parameter Predictor.

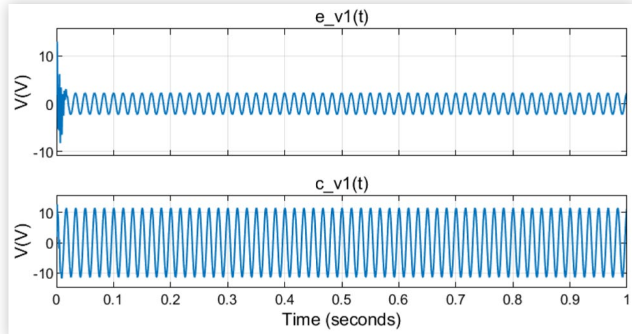

FIGURE 17 State Tracking Error and Coupling Error for Control Signal of the Controlled Current Source 1 in 1-Parameter Predictor.

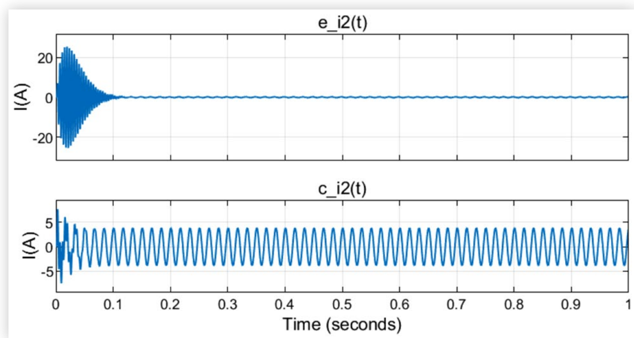

for one-parameter and two-parameter systems. Figure 17 and Figure 18 illustrate the state and coupling errors for the sent voltage $i_1(t)$ prediction system for one-parameter and two-parameter systems. Figure 19 and Figure 20 illustrate the state and coupling errors for the sent voltage $v_2(t)$ prediction system for one-parameter and two-parameter systems. It is important to note that the additional tunning parameter β leads to different state tracking errors and coupling errors. The plot in Figures 15, 16, 17, 18, 19, and 20 reveal that for the additional

FIGURE 18 State Tracking Error and Coupling Error for Control Signal of the Controlled Voltage Source 2 in 2-Parameter Predictor.

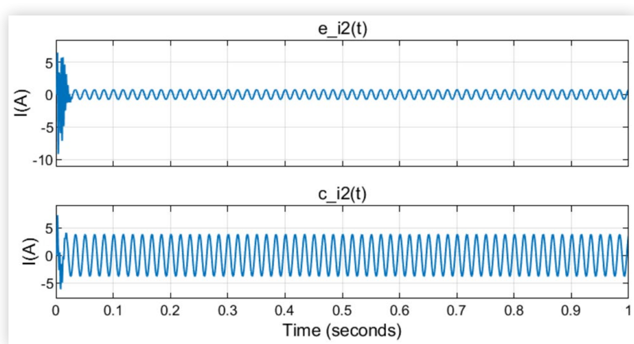

FIGURE 19 State Tracking Error and Coupling Error for Control Signal of the Controlled Voltage Source 1 in 1-Parameter Predictor.

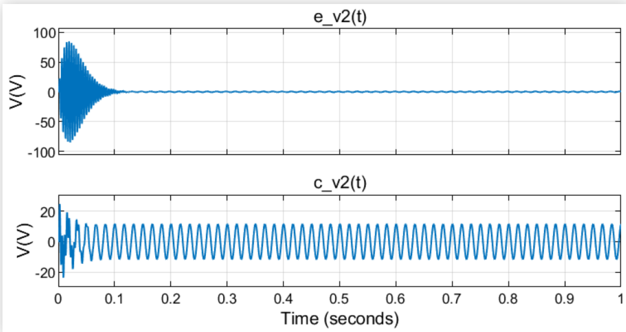

FIGURE 20 State Tracking Error and Coupling Error for Control Signal of the Controlled Voltage Source 1 in 2-Parameter predictor.

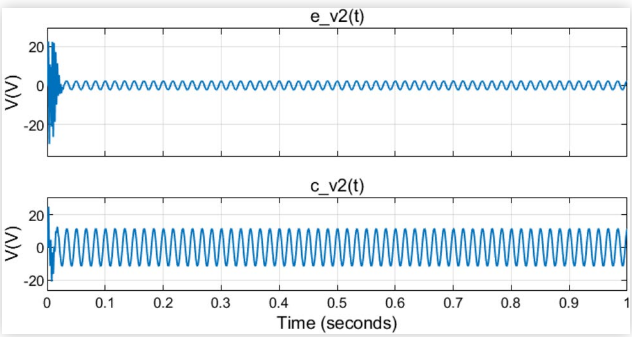

tunning parameter β, the predictor produces a quicker state-tracking response. Additionally, in steady state, the ratio between the state tracking error's magnitude and coupling error magnitude becomes smaller, which agrees with the stability analysis earlier presented in the Bode plot. This finding further supports the effectiveness of the predictors, especially the two-parameter version, in enhancing the system's state-tracking performance.

The Nyquist plot for the different interface algorithms shows the superiority of the damped impedance method over the ideal transformer model and partial circuit duplication. These plots identify the limitations of these interface algorithms in the power system and the choice of DIM. This ensures system stability, preservation of simulation fidelity, and system robustness. The two-parameter predictor framework improves the delay compensation performance of the predictor while maintaining its model-free nature. Figures 14–19 show that an additional degree of freedom can help improve prediction accuracy in the three coupling signals of the damped impedance interface algorithms used in power system co-simulation.

Summary/Conclusions

The one-parameter and two-parameter model-free predictor framework deal with communication delays in a power system partitioned into two subsystems for co-simulation. These predictors have been applied to the three interface coupling signals of the damped impedance method of interface algorithms. The use of damped impedance as an interface algorithm is justified by the Nyquist plot of the transfer function to check the point at which the ratio of the subsystem impedances encircles the point (-1+0j). A stability analysis is conducted to establish the relationship between the tunning parameters and the predictor's stability. Through transient performance, the one-parameter and two-parameter predictors are implemented to validate predictor design and analysis. The predictors, especially the two-parameter version, have significant potential to reduce the negative effect of delays. The predictors perform better at lower frequencies as having an additional degree of freedom may come with a trade-off between improved performance in one area and a compromise in another. Specifically, in this case, the trade-off is between having more design flexibility and the risk of increased oscillations in the error gain at high frequencies. Thus, it is recommended to decompose signals into quantities that vary less with time before the prediction is applied at high frequencies. The two-parameter predictor design offers certain advantages over the single-parameter predictor. The former design provides an increased potential for delay compensation and expands the operational stability of the predictor. This implies that the two-parameter design provides more flexibility in compensating for delays and enables the predictor to operate in a wider range of conditions without becoming unstable. However, it should be noted that introducing the second parameter results in oscillatory error gain at high frequencies, which is a drawback of the design.

References

1. Hoang, P.H., Ozkan, G., Badr, P.R., Timilsina, L. et al., "Integrating Degradation Forecasting into Distribution Grids' Advanced Distribution Management Systems," *Int. J. Electr. Power Energy Syst.* 150 (2023): 109071, doi:10.1016/j.ijepes.2023.109071.
2. Hoang, P.H., Ozkan, G., Badr, P., Timilsina, L. et al., "A Prognostic Based Control Framework for Hybrid Electric Vehicles," SAE Technical Paper 2022-01-0352 (2022), doi:https://doi.org/10.4271/2022-01-0352.
3. Stevic, M., Estebsari, A., and Vogel, S., "Multi-Site European Framework for Real-Time Co-Simulation of Power Systems," *IET Gener. Transm. Distrib.* 11 (2017): 4126-4135, doi:10.1049/iet-gtd.2016.1576.
4. Arsalan, A., Ahmad, J., Tahir, M. and Mazumder, S.K., "Distributed Control and Power Management of Islanded DC Nanogrids with Applications to Rural Electrification," in *2020 IEEE Energy Conversion Congress and Exposition (ECCE)* 2020, 4662-4667, doi:10.1109/ECCE44975.2020.9236352.
5. Syed, M.H., Guillo-Sansano, E., Wang, Y., Vogel, S. et al., "Real-Time Coupling of Geographically Distributed Research Infrastructures: Taxonomy, Overview, and Real-World Smart Grid Applications," *IEEE Trans. Smart Grid* 12 (2021): 1747-1760, doi:10.1109/TSG.2020.3033070.

6. Liu, R., Mohanpurkar, M., Panwar, M., Hovsapian, R. et al., "Geographically Distributed Real-Time Digital Simulations Using Linear Prediction," *Int. J. Electr. Power Energy Syst.* 84 (2017): 308-317, doi:10.1016/J.IJEPES.2016.06.005.
7. Monti, A., Stevic, M., Vogel, S., De Doncker, R.W. et al., "A Global Real-Time Superlab: Enabling High Penetration of Power Electronics in the Electric Grid," *IEEE Power Electron. Mag.* 5 (2018): 35-44, doi:10.1109/MPEL.2018.2850698.
8. Mirz, M., Estebsari, A., Arrigo, F., Bompard, E. et al., "Dynamic Phasors to Enable Distributed Real-Time Simulation," in *Proceedings of the 2017 6th International Conference on Clean Electrical Power: Renewable Energy Resources Impact, ICCEP 2017*, 2017, 139-144.
9. Timilsina, L., Badr, P.R., Hoang, P.H., Ozkan, G. et al., "Battery Degradation in Electric and Hybrid Electric Vehicles: A Survey Study," *IEEE Access* 11 (2023): 42431-42462, doi:10.1109/ACCESS.2023.3271287.
10. Ersal, T., Brudnak, M., Salvi, A., Stein, J.L. et al., "Development and Model-Based Transparency Analysis of an Internet-Distributed Hardware-in-the-Loop Simulation Platform," *Mechatronics* 21 (2011): 22-29, doi:10.1016/j.mechatronics.2010.08.002.
11. Guo, S., Liu, Y., Zheng, Y., and Ersal, T., "A Delay Compensation Framework for Connected Testbeds," *Cybern. Syst.* 52 (2022): 4163-4176, doi:10.1109/TSMC.2021.3091974.
12. Stevic, M., Estebsari, A., Vogel, S., Pons, E. et al., "Multi-Site European Framework for Real-Time Co-Simulation of Power Systems," *IET Gener. Transm. Distrib.* 11 (2017): 4126-4135, doi:10.1049/iet-gtd.2016.1576.
13. Faruque, M.O., Strasser, T., Lauss, G., Jalili-Marandi, V. et al., "Real-Time Simulation Technologies for Power Systems Design, Testing, and Analysis," *IEEE Power Energy Technol. Syst. J.* 2 (2015): 63-73, doi:10.1109/JPETS.2015.2427370.
14. Liu, R., Mohanpurkar, M., Panwar, M., Hovsapian, R. et al., "Geographically Distributed Real-Time Digital Simulations Using Linear Prediction," *Int. J. Electr. Power Energy Syst.* 84 (2017): 308-317, doi:10.1016/j.ijepes.2016.06.005.
15. Brandl, R., "Operational Range of Several Interface Algorithms for Different Power Hardware-in-the-Loop Setups," *Energies* 10 (2017), doi:10.3390/en10121946.
16. Syed, M.H., Guillo-Sansano, E., Blair, S.M., Avras, A. et al., "Synchronous Reference Frame Interface for Geographically Distributed Real-Time Simulations," *IET Gener. Transm. Distrib.* 14 (2020): 5428-5438, doi:10.1049/iet-gtd.2020.0441.
17. Zhang, Z., Fickert, L., and Zhang, Y., "Power Hardware-in-the-Loop Test for Cyber Physical Renewable Energy Infeed: Retroactive Effects and an Optimized Power Hardware-in-the-Loop Interface Algorithm," in *Proceedings of the Proceedings - 2016 17th International Scientific Conference on Electric Power Engineering, EPE 2016*, 2016, 1-6. IEEE.
18. Guo, S., Liu, Y., Zheng, Y., and Ersal, T., "A Delay Compensation Framework for Connected Testbeds," *IEEE Trans. Syst. Man, Cybern. Syst.* 52 (2022): 4163-4176, doi:10.1109/TSMC.2021.3091974.
19. Zheng, Y., Brudnak, M.J., Jayakumar, P., Stein, J.L. et al., "A Predictor-Based Framework for Delay Compensation in Networked Closed-Loop Systems," *IEEE/ASME Trans. Mechatronics* 23 (2018): 2482-2493, doi:10.1109/TMECH.2018.2864722.
20. Ge, X., Zheng, Y., Brudnak, M.J., Jayakumar, P. et al., "Analysis of a Model-Free Predictor for Delay Compensation in Networked Systems," 7 (2017): 201-215, doi:10.1007/978-3-319-53426-8_14.
21. Buraimoh, E. and Davidson, I.E., "Fault Ride-Through Analysis of Current- and Voltage-Source Models of Grid Supporting Tour Des Défaillances Par Analyse Des Modèles de Source de Courant et de Tension d' Un Réseau Supportant Un Micro-Réseau d' Onduleur," *IEEE Can. J. Electr. Comput. Eng. Can. Genie Electr. Inform.* 44 (2021): 189-198.
22. Buraimoh, E. and Davidson, I.E., "Simplified LCL Filter State Space Modeling and Small Signal Stability Analysis of Inverter Based Microgrid," in *Proceedings of the 2021 IEEE PES/IAS PowerAfrica, PowerAfrica 2021*, August 23, 2021, 1-5. Institute of Electrical and Electronics Engineers Inc.

Contact Information

Contact details for the main author should be included here. Details may include mailing address, email address, and/or telephone number (whichever is deemed appropriate).

Acknowledgments

This work was supported by Clemson University's Virtual Prototyping of Autonomy Enabled Ground Systems (VIPR-GS), under Cooperative Agreement W56HZV-21-2-0001 with the US Army DEVCOM Ground Vehicle Systems Center (GVSC).

DISTRIBUTION STATEMENT A. Approved for public release; distribution is unlimited. (OPSEC 7578).

ISSN 0148-7191